The Cryosphere Discuss., https://doi.org/10.5194/tc-2018-45
Manuscript under review for journal The Cryosphere
Discussion started: 15 March 2018

The Cryosphere Discussions
Open Access
EGU

Mechanisms leading to the 2016 giant twin glacier collapses, Aru range, Tibet

Adrien Gilbert[1], Silvan Leinss[2], Jeffrey Kargel[3,4], Andreas Kääb[1], Tandong Yao[5], Simon Gascoin[6], Gregory Leonard[3], Etienne Berthier[7] and Alina Karki[8]

[1]Department of Geosciences, University of Oslo, Norway
[2]Institute of Environmental Engineering, ETH Zurich, Zurich, Switzerland
[3]Department of Hydrology and Atmospheric Sciences, University of Arizona, USA
[4]Planetary Science Institute, University of Arizona, USA
[5]ITP-CAS, Beijing, China
[6]CESBIO, CNES, CNRS, IRD, UPS, Université de Toulouse, Toulouse, France
[7]LEGOS, CNES, CNRS, IRD, UPS, Université de Toulouse, Toulouse, France
[8]Society for Ecological Restoration-Nepal, Kathmandu, Nepal

Correspondence to: Adrien Gilbert (adrien@geo.uio.no)

Abstract. In northwestern Tibet (34.0°N, 82.2°E) near lake Aru Co, the entire ablation area of two glaciers (Aru-1 and Aru-2) suddenly collapsed on 17 July 2016 and 21 September 2016, respectively, and transformed into 68 and 83 10^6 m^3 mass flows that ran out up to 7 km, killing nine people. The only similar event currently documented is the 2002 Kolka Glacier mass flow (Caucasus Mountains). Using climatic reanalysis, remote sensing and 3D thermo-mechanical modeling, we reconstructed in detail the glaciers' thermal regimes, thicknesses, velocities, basal shear stresses and ice damage prior to the collapse. We show that frictional change leading to the collapses occurred in the temperate areas of polythermal glacier structures and are not linked to thaw of cold based ice. The two glaciers experienced a similar stress transfer from predominant basal drag towards predominant lateral shearing in the later detachment areas and during the 5-6 years before the collapses, though with a high friction patch on Aru-2 tongue which is inexistent on Aru-1. The latter led to distinctly disparate behaviour making the development of the instability more visible for the Aru-1 glacier compared to Aru-2 through enhanced crevassing over a longer period and terminus advance. Field investigations reveal that those two glaciers are flowing on a soft, highly erodible, and fine-grained sedimentary lithology. We propose that specific bedrock lithology played a key role in the two Tibet, and also in the Caucasus gigantic glacier collapses documented to date by producing low bed roughness and large amount of till rich in clay/silt with low friction angle. The twin Aru collapses would have been driven by a failing substrate linked to increasing water pore pressure in the subglacial drainage system in response to recent increases of surface melting and rain.

The Cryosphere Discuss., https://doi.org/10.5194/tc-2018-45
Manuscript under review for journal The Cryosphere
Discussion started: 15 March 2018

1. Introduction

In the Aru mountain range on the Western Tibetan Plateau, on July 17 2016, the entire ablation zone of a nameless glacier (termed here Aru-1) spontaneously collapsed despite its low slope angle (13°) (Tian et al., 2016) compared to classical ice avalanches sourced from hanging glacier failure (Faillettaz et al., 2015). It produced a high-speed ice avalanche exceeded 200 km h^{-1} and spread out over a 7 km long and 3 km wide deposit, killing nine people (Kääb et al., 2018). This event was followed by the collapse of the closest glacier south to Aru-1 two months later, on 21 September 2016, producing a similar low-slope angle gigantic avalanche (see Figure 1B). These catastrophic collapses are unique by their size and mobility. Only one similar case has been documented before, the Kolka/Karmadon glacier collapse in the Caucasus mountains in 2002 (Evans et al., 2009; Huggel et al., 2005). In order to anticipate potential similar hazards in other populated mountain areas we need to understand in detail the mechanisms and identify potential triggers and factors responsible for these extreme events. Among others, such collapses raise the question of their occurrence in the future with respect to the on-going climate change.

Applying satellite imagery analysis and mass balance modeling, Kääb et al. (2018) explored the long-term behaviour of the two glaciers leading to the collapse. They show that the two collapsed glaciers started a surge-like instability around 2010, probably in response to both increasing precipitation and temperature in the region. Their preliminary analysis of the 2D thermal regime shows a polythermal structure for the two glaciers that would have played a role in the collapses by providing downstream resisting forces against sliding and promoting englacial drainage to the bed only in the lower part of the accumulation zone. Facing the enigma of two neighbouring glaciers undergoing a similar behaviour that otherwise is globally almost unique, Kääb et al. (2018) also point out the possible role of a specific bedrock lithology and glacier till in the reducing of glacier basal friction involved in the instability.

In this study, we significantly extend the quantitative analysis and discuss in detail the mechanisms leading to the collapses. We used a 3D full-Stokes thermo-mechanical model in order to (i) reconstruct the bedrock topography, (ii) analyze in 3D the thermal regime, (iii) infer the evolution of the basal friction prior to the collapse, and (iv) quantify the stress distribution that led to the final collapses. We then combine the modeling results with field investigations to further develop the role of bedrock lithology and discuss the origin of the twin collapse. Finally, we provide key-characteristics to recognize similar lithologic and thermal regimes for other glaciers.

2. Observations

The Aru range is located on the remote Western Tibetan plateau (34°N, 82°E) where very few glaciological or meteorological observations are available (Figure 1). Prior to Kääb et al. (2018), the two collapsed glaciers were never studied before and the entire modeling work of this study is therefore based on remote sensing data and climatic reanalysis. DEM differencing provided both observations on the glacier transient dynamics and mean mass balance over different time periods needed to calibrate the model. Kääb et al. (2018) compared different sources of local climatic data in order to reproduce remote sensing based mass balance observation and concluded that ERA-interim reanalysis provides the best estimate of the Aru range climate,

if the respective precipitation amounts are corrected by a multiplying factor of about 4. We use here their mass balance model for constraining the thermo-mechanical model described in section 3.2.

2.1. Digital Elevation Models (DEMs)

We used seven different DEMs derived from different satellite missions between 2000 and 2016 (see Table 1). The SRTM C-band DEM from mid-February 2000 (Farr et al., 2007) was used as the steady-state reference of the two glaciers for reconstructing bedrock topography. A Pléiades satellite stereo DEM from 1 October 2016 after the collapse allows us to, in parts, validate the modeled bedrock reconstruction over the detachment zone. We computed emergence velocities by differencing pre-collapse high resolution DEMs from Tandem-X, Spot7 and Worldview imagery and correcting these for mass balance following the approach described in Gilbert et al. (2016) (Figure 2). Uncertainty linked to radar penetration should be limited when comparing same wavelength (band-X) since penetration length would be similar between the two images. Comparing Spot7 (2015) and Tandem-X (2014) likely introduce uncertainty in the accumulation area leading to higher emergence velocities in this part (visible in Figure 3). This only influence our friction reconstruction in the higher part of the glacier and not on the detachment area. Details on DEM accuracies and acquisition methods can be found in Kääb et al. (2018).

2.2. Field observations

We investigated glacier till properties by analyzing samples collected from the Aru-1 avalanche deposit in the gorge close to the former glacier tongue. We collected these samples one year after the collapse on 18 July 2017. Rainy conditions on that day highlighted the behaviour of the surrounding lithology that quickly turned to soft and unstable slurries in the presence of water. Additional information about our samples can be found in supplementary material to this article (Figures S3 to S5).

3. Modeling methods

3.1. Mass Balance

Our mass balance model for the two Aru glaciers is based on a degree-day model described in Gilbert et al. (2016). It has been calibrated in using satellite-derived glacier mass balance and is fed by ERA-interim climate reanalysis (Kääb et al., 2018). The model output provides the spatial distribution of surface mass balance, firn thickness, and available surface melt water for percolation/refreezing in the firn to constrain the thermo-mechanical model.

3.2. Thermo-mechanical model

Our thermo-mechanical ice-flow model is based on the Stokes equation coupled with an energy equation using the enthalpy formulation (Aschwanden et al., 2012; Gilbert et al., 2014). Changes in the glacier geometry are computed using a free surface

equation (Gilbert et al., 2014). We adopt a pure viscous isotropic ice rheology following Glen's flow law (Cuffey and Paterson, 2010). The model is solved using the finite-element software Elmer/ice (Gagliardini et al., 2013).

We adopt a linear friction law as a basal boundary condition for the Stokes equation that reads:

$$\tau_b = \beta u_s \qquad (1)$$

where τ_b is the basal shear stress (MPa), u_s is the sliding velocity (m yr^{-1}) and β the friction coefficient (MPa yr m^{-1}). This coefficient is inverted using a control inverse method to minimize a cost function defined from the misfit with measured surface data and a regularization term (Gagliardini et al., 2013; Gillet-Chaulet et al., 2012). Following Gilbert et al. (2016) we used here the surface-normal velocity U_{Nz}^{obs} (m yr^{-1}) to compute this cost function. This velocity is obtained by removing the mean modeled mass balance from the elevation change rate measured from our repeat satellite-derived DEMs over the same periods (Figure 2).

The surface boundary condition is set as a stress-free boundary for the Stokes problem and using a Dirichlet condition for the enthalpy equation. In order to take into account water percolation and refreezing within the firn, we follow the approach by Gilbert et al. (2015), in this case using a 6-month time step. Latent heat due to refreezing is released every year during a time steps that includes summer. The firn-thickness distribution is estimated from the mass balance model following Gilbert et al. (2016) and the firn density is computed using a linear density profile set to:

$$\rho(y) = \rho_0 + \frac{d}{H_{firn}}(\rho_{ice} - \rho_0) \qquad (2)$$

where ρ is the density (kg m^{-3}) at depth d (m), ρ_0 is the surface density, ρ_{ice} is the ice density and H_{firn} the firn thickness (m).

The lateral boundary condition is set to a no-flux condition for both the Stokes and enthalpy equations. We assume a basal heat flux of 8.0 10^{-2} W m^2 for the enthalpy equation according to heat flux measured in boreholes at Guliya ice cap (6200 m a.s.l., 200 km north to Aru range) (Thompson et al., 1995) and geothermal heat flux modeled in the region (Tao and Shen, 2008).

3.3. Modeling strategy for the steady state glaciers

The first step of modeling the dynamics and thermal regime of the Aru glaciers is to obtain a steady-state glacier as initial condition for 1970 (start of the climatic reanalysis used). Landsat satellite images of the glacier area and the mass balance model suggest that the two glaciers were close to equilibrium from 1970 to 1995) (Kääb et al., 2018). We therefore assume that the surface topography measured in February 2000 by the SRTM mission (oldest available DEM) is representative of the glaciers being in equilibrium with the mean climate over this period, although the positive mass balance between 1995 and 2000 probably thickened the glacier by a few meters in the accumulation area. We use the mean mass balance between 1980

and 1995 as an equilibrium mass balance considering that modeled mass balance is close to steady state during this period before becoming positive from 1995 to 2008 (Kääb et al., 2018).

We first run the model on a 2D flow line until a steady state is reached, using the Pléiades DEM from after the collapses as bedrock topography in the detached parts and by reconstructing the bed at the higher glacier parts assuming a constant basal shear stress (plastic approximation, see Cuffey and Paterson (2010)). This initial step allows for the first approximation of the steady-state thermal regime which we presented already in Kääb et al. (2018). We use then the 10m-depth temperature modeled by the flow line model to define the steady-state surface enthalpy as a function of elevation which include meltwater percolation and refreezing effects. This relationship is used to define a Dirichlet surface boundary condition for enthalpy in order to solve the steady-state thermal regime of the glacier in 3D in the bedrock inversion procedure (section 3.3.1). Because the effect of meltwater percolation and refreezing is already included in the surface enthalpy value, it avoids solving meltwater percolation and refreezing in diagnostic runs. The final 3D steady state glacier is properly obtained at the end by running a transient simulation using the inverted bedrock topography and solving water percolation and refreezing until surface topography and enthalpy field reach equilibrium with the imposed climatic condition.

3.3.1. Reconstructing bedrock topography

Using constant climatic conditions associated with the balanced glacier conditions for the SRTM DEM, we determined the bedrock topography allowing the best match between modeled and observed (i.e., SRTM DEM) surface topography (van Pelt et al., 2013). For this purpose, we run a 3D transient simulation assuming no sliding, fixed surface topography (SRTM DEM), and constant surface forcing (mass balance and enthalpy). Mesh horizontal resolution is set to about 50 m with 15 vertical layers. The evolution of the free surface is taken into account by varying the basal mesh elevation instead of the surface elevation. The mesh surface topography remains thus constant while the bed topography is updated by solving the equation

$$\frac{\partial(z_{bed})}{\partial t} + \overrightarrow{v_s} \cdot \vec{\nabla}(z_{bed} - z_{bed0}) = \overrightarrow{v_s} \cdot \vec{\nabla} z_{s0} - MB - w_s \quad (3)$$

where z_{bed} is the bedrock elevation (m), $\overrightarrow{v_s}$ is the surface horizontal velocity (m yr^{-1}), z_{bed0} is the initial bedrock topography (m), MB is the surface mass balance (m yr^{-1}), w_s the vertical component of the surface velocity (m yr^{-1}) and z_{s0} is the measured surface elevation (m). The right side of Eq. 3 vanishes once bedrock topography satisfies the required topography to keep z_{s0} constant for a given mass balance MB. The advective term in the left side of Eq. 3 allows smoothing z_{bed} in the flow direction. The enthalpy field is solved at each time step by solving the steady-state equation for the current velocity field and mesh. We initially start with a uniform 200 m ice thickness (rough maximum expected thickness on the glacier) and run the model until reaching steady bedrock topography. This gives a new z_{bed0} value to start again the procedure until reaching a new steady state. After only two iterations, we validate the modeled bedrock topography by running the model with the fixed new inferred

bedrock topography and free surface evolution. The resulting surface topography is in excellent agreement with the measured one (Figure 3) meaning that our method to infer the bedrock topography works well in these two cases.

We use the opportunity provided by the detachments to compare the reconstructed bedrock topography with the measured Pléiades DEM from after the collapses (Figure 3). On Aru-2, the points where the bedrock is clearly visible in the Pleiades image match well with the locations where our reconstructed bedrock topography matches the Pléiades DEM (dots in Fig. 3). Elsewhere in the Aru-2 detachment zone the modeled bedrock is deeper than the observed surface elevation, but this is likely due to the remaining ice debris so that the Pléiades DEM is higher than the actual bedrock. On Aru-1, the reconstructed bedrock on profiles 2, 3 and 4 is systematically deeper than the Pléiades DEM, even on the steep side close to the margin of the glacier where no ice remained after the collapse. This means that ice flow is not accurately modeled in this part likely due to the premise of no sliding, which is probably not accurate considering that the glacier may be temperate at its base here (see section 4.1). This should also affect the result on Aru-2, which has a similar thermal regime, but where the no-sliding condition seems to work. This indicates the existence of different sliding conditions in the two glaciers prior to collapse, as also supported by the friction inversion analysis presented in section 4.2.

4. Results

4.1. Steady state configuration of the two glaciers

The Aru glaciers are representative of a cold and semi-arid climate regime and show little dynamics under mostly cold ice conditions. The steady-state equilibrium line is located around 5750 m a.s.l. with a maximum accumulation of 0.6 m w.eq. yr^{-1} at 6100 m a.s.l. and a maximum ablation of -2.5 m w.eq. yr^{-1} on the tongue (Figure 4B). Both glaciers are composed of two similar catchments characterized by a smaller western branch that joins the main stream in the ablation area. The western branch of each glacier is thinner and is less dynamic compared to the main branches that collapsed in summer 2016 (Figure 4A). Maximum surface horizontal velocity reached 20 m yr^{-1} in Aru-2, which is thicker than Aru-1 due to a wider accumulation area (1.7 km^2 vs 1.2 km^2) converging in a similarly narrow gorge.

As previously concluded by Kääb et al. (2018), our results show that the main branches of the two glaciers are characterized by a polythermal structure with a cold accumulation zone above 5900 m a.s.l. and a temperate based ablation area surrounded by cold ice (Figure 5). However, thanks to a more accurate bedrock topography and a 3D approach, we show here that the temperate parts likely extend in significantly larger areas beneath the detachments than previously though. Temperate ice forms in the lower part of accumulation zone due to a significant amount of percolation and refreezing of melt water, which increase the temperature of the near-surface firn. This warmer ice is then advected into the ablation zone contributing, together with basal heat flux, to create a temperate basal condition in the deeper parts of each glacier. Cold surface conditions due to absence of water percolation in the ablation zone (cold impermeable ice) lead to a significant surface cold layer that eventually reaches the glacier base in the shallowest region (Figure 5). The western branches of the two glaciers have a significantly smaller temperate area with an ablation zone almost entirely cold-based (Figure 5). This thermal structure explains why the western

branches remained stable after the collapses even though each branch lost its downstream supporting buttresses formed by the collapsed glacier tongues. The modeled spatial extent of the temperate basal ice coincides with the detached area and suggests that friction changes leading to the collapse occured in temperate ice rather than being produced by a thermal change from cold to temperate conditions. However, the large amount of cold ice, especially along the side of the gorge, could have provided significant lateral drag that built up high driving stress able to balance gravitational force in case of friction change in the temperate core.

4.2. Friction change at the glacier base over the last 5 years before the collapse

The surge-like behaviour of the two glaciers identified from DEM comparison in Kääb et al. (2018) documents a change in the glacier dynamics during the five years prior to the twin collapses. By removing the elevation change due to surface mass balance we quantified the surface-normal velocity for constraining the basal friction parameter (Gilbert et al., 2016) on different periods: 2011-2013, 2013-2014, 2014-2015 and September/November 2015 (see Table 1 and Figure 2). Our results highlight a contrasting behaviour between Aru-1 and Aru-2 where friction decreased progressively in magnitude through time in both glaciers, but over significantly different areas (see Figure 6). Frictional changes over the five years prior to collapse are also more significant on Aru-1, resulting in a higher increase in surface velocity than on Aru-2 (Figure 7). Similar inferred friction for Aru-2 for annual means (2011-2013 or 2013-2014) and a 2-month mean (Sept/Nov 2015) suggests low seasonal variability of the basal condition. Similarly, modeled surface velocities on Aru-1 in Sept/Nov 2015 correlate well with those measured for Jan/Apr 2016 by satellite image correlation (Kääb et al., 2018) (Figure 7f), also suggesting low seasonal variability.

4.3. Force balance analysis

To evaluate how resisting forces acted and evolved to balance the driving forces, we computed the mean basal shear stress during different periods from the inverse method. Thereby we assumed that basal shear stress is mainly constrained by the global stress balance and should not be influenced by the sliding law that we used (eq. 1) (Joughin et al., 2004; Minchew et al., 2016). The steady-state condition shows a basal shear stress between 100 kPa and 200 kPa in both glaciers with a mean shear stresses of 137 kPa and 150 kPa for Aru-1 and 2, respectively (Figure 8A). In comparison, mean driving stresses are 152 kPa (Aru-1) and 213 kPa (Aru-2) meaning that 10% (Aru-1) and 30% (Aru-2) of the driving force is accommodated by normal force along the sidewalls. This driving stress is at the higher end of the observed range of driving stresses on mountain glaciers (Cuffey and Paterson, 2010) and reflects the presence of strong resisting forces due to mainly cold-ice conditions combined with the resistance of the valley walls.

The inversion from mean elevation changes between September and November 2015 (Figure 8B) reveals that basal shear stress on Aru-1 decreased to only 20 to 10 kPa in large areas and basal resistance on the detachment zone became mainly achieved by a few sticky spots (Stokes et al., 2007) where shear stress exceeded 250 kPa. On the external side of the curve which both glaciers form, close to the terminus of Aru-1, shear stress is about 6-7 kPa and was not more than 15 kPa at the terminus. In

comparison, Aru-2 behaves differently with more localized friction changes that produce smaller change in the distribution of the basal shear stress during the same period (Figure 8C).

The analysis of the dynamics and force balance evolution on an area restricted to the detachment zone (dashed lines in Figure 8) reveals both similarities and differences between the two events (Figure 9). On the one hand, as already highlighted in Figure 7, the mean detachment velocity prior to collapse behaved differently for the two glaciers (Figure 9A). While the Aru-1 detachment significantly accelerated following behaviour typical for slope failure (Voight, 1990) over several years (blue dashed line in Figure 9A), Aru-2 shows very little acceleration. On the other hand, force balances evolved similarly in the two detachments with a large increase of lateral stresses due to both driving stress increasing and basal friction reducing (Figure 9B). Interestingly, lateral resistance overcomes basal resistance in both detachments with a delay (81 days) close to the delay between the two final collapses, 66 days (Figure 9C). On Aru-2, it seems that smaller changes in friction are compensated by a higher change in driving stresses resulting in a similar increase of stress at the detachment margin compared to Aru-1 (Figure 9B). The difference in surface velocity response to these similar stress transfers relies on a different basal drag repartition in the two glaciers. Basal drag decreased uniformly on the whole detachment of Aru-1 with the appearance of localized sticky spots whereas drag decreased only in the higher part of the detachment of Aru-2. This led to more intense bulging and a lower velocity increase (Kääb et al., 2018) due to the high-friction patch remaining in the tongue (Figure 6).

To evaluate the impact of the friction change on the mechanical property of the ice, we compute the maximal principal Cauchy stress and compare it with a threshold value (set to 0.1 MPa (Krug et al., 2014)) to identify the damage production (crevasse opening) (Krug et al., 2014; Pralong and Funk, 2005) (Figure 10). This clearly highlights a progressive intensification of cracks opening around the detachment zone of Aru-1 (Figure 10C) as observed on satellite images (Kääb et al., 2018) that led to the final collapses. In comparison, Aru-2 behaves again differently with less damage that only affects the upper part on the detachment (Figure 10C). This means that sudden damage of the shear margin would had to occur in Aru-2 in 2016 which is confirmed by the observed sharp crack surrounding the detachment a few days before the collapse (Kääb et al., 2018). In sum, Aru-1 and Aru-2 underwent a similar stress transfer from basal drag to lateral shearing in their respective detachments, but with different responses in terms of damage and sliding speed due to different basal drag repartition. Aru-1 progressively evolved towards collapse whereas Aru-2 accumulated stresses until a sudden release led to collapse. This indicates that critical stress transfers, precursory to the collapses, may occur without observable phenomena (i.e., surface velocity increase) in the preceding years.

5. Discussion

5.1. Result uncertainties

The modeled thermal regime is sensitive to basal heat flux, which is poorly constrained. However, sensitivity test (see supplementary material, Figure S1) show that the temperate area remains similar for a basal heat flux comprised between 6.0 10^{-2} and 1.2 10^{-1} W m^{-2} and disappear at 2.0 10^{-2} W m^{-2}. Measurement in Guliya Ice Cap (Thompson et al., 1995) and

reconstruction from Tao and Shen (2008) both give a value of 8.0 10^{-2} W m^{-2} making a low value of 2.0 10^{-2} W m^{-2} very unlikely. Also, modeled thermal regime and friction reconstruction, which are almost independent, show a good accordance between the localization of sliding and modeled temperate areas giving confidence in our results (see section 5.2).

The basal friction reconstruction mainly depends on measured elevation change accuracy, which is higher over long time-period making the 2011-2013 reconstruction the more reliable. The measured September/November 2015 elevation change is subject to higher nose level and is poorly resolved in the accumulation area (see Figure 2) making the reconstruction more reliable on the detachment area where elevation change are significant. Same conclusion applies to the 2014-2015 reconstruction where the higher part of the glacier is affect by penetration of the band-X leading to an overestimation of the surface-normal velocities. The influence of uncertainty in the modeled mass balance used to compute surface-normal velocity is also low in the detachment part since elevation change due to surface mass balance are small compared to dynamical height change linked to the instability (<20%). This makes our results reliable, at least in the detachment area, which is the focus of the study.

5.2. Frictional changes

Our results suggest that low friction below the Aru glaciers is not linked to seasonal variability of water pressure that is often observed on glaciers elsewhere (Bartholomaus et al., 2008; Vincent and Moreau, 2016). Rather, it is likely associated with sustained change of the basal condition caused by an accumulation of liquid water over several years prior to the collapse. Over a hard bed (Cuffey and Paterson, 2010), this would mean the existence of a subglacial lake which is very unlikely here because low friction on Aru-1 reaches the tongue and the lake should have drained in such case. Futhermore, in temperate ice, high water pressure conditions are unstable over long time periods because they lead to channel formation that can efficiently decreases the pressure (Schoof, 2010). High water pressure in a cavity network would be also difficult to maintain in the Aru cases since increasing sliding speeds tends to increase cavity size and decrease water pressure. These results suggest that basal friction under the Aru glaciers was probably controlled by processes associated with soft bed properties (Cuffey and Paterson, 2010).

Comparison between sliding speed evolution and modeled basal steady-state temperature reveals a good correlation between zone of sliding and temperate ice and show that the size of sliding areas remain similar during time (Figure 11). This confirms that friction reduction since 2011 mainly occurred within zones that are already temperate areas and is therefore not linked to a change from temperate to cold basal conditions. However, contrary to Aru-1, Aru-2 appears to have been affected by a high-friction zone under its lower tongue that modeled basal temperatures do not explain as it indicates there temperate conditions, not cold ones (Figure 11). This zone of high friction explains the different behaviour between the two glaciers in terms of surface velocities and glacier advance. Indeed, a few months before the collapse, Aru-2 velocities were still very low compared to Aru-1 (Figure 7) and although Aru-1 advanced almost 200 m since July 2015, the front of Aru-2 remained unchanged until

the collapse (Kääb et al., 2018). The high friction zone may have delayed the collapse of Aru-2 but it did not prevent it. The origin of this high friction zone is discussed at the end of section 5.2.

5.3. Role of the bedrock lithology and glacier till

Field observations after collapse, and inspection of the detachment zones showed no presence of a hard-bed lithology beneath the glacier, and no large boulders were observed in the forefields. Rather, extensive deposit of soft, unconsolidated and fine-grained lithologies were identified (see supplementary material, Figures S3 to S5). We collected till samples from the avalanche Aru-1 deposit and measured their grain-size distribution (Figure 12). Mean values over the four samples in the avalanche path (Fig. 12) give 14% clay, 24% silt, 44% sand and 18% gravel. These samples are representative of the material found in the deposit and are likely also representative of the glacier till on which the glacier rested. We also observed low bedrock roughness at macro scale (>1m).

These findings confirms that the Aru glaciers flowed on a soft-bed, which may have played an important role in controlling the behaviour of the Aru glaciers from the surge initiation to the final collapse. For such bed type, basal motion is not controlled by ice flow around bedrock bumps (Lliboutry, 1968; Weertman, 1964) but rather by deformation in the till (Truffer et al., 2001). The sustained very low basal drag under Aru glaciers (<20kPa) may be similar to ice stream mechanisms whereby water-saturated till enables fast flow at low driving stresses (≈20kPa) (Cuffey and Paterson, 2010). It has been shown that glacier till behaves with a plastic rheology with a shear strength strongly dependent on the effective normal stress (Clarke, 2005; Iverson et al., 1998; Iverson, 2010; MacAyeal, 1992). Such behaviour was found to be well described by a Coulomb-type friction law (Boulton and Jones, 1979; Clarke, 2005; Tsai et al., 2015) as follows:

$$\tau_u = c + N\tan(\phi) \qquad (4)$$

where τ_u is the ultimate shear strength, c the cohesion parameter, N the normal effective stress and φ the friction angle. This kind of law where shear stress is independent of the sliding velocity allows unstable behaviour leading to failure. In a general case, glaciers remains stable because till and water pressure are not equally distributed at the basal interface leading to sticky spots where stress concentrates to balance gravitational forces together with lateral drag at glacier margins (Cuffey and Paterson, 2010). The Aru collapses would thus be an example where the till plastic rheology becomes the only source of resisting forces to balance gravity, eventually leading to catastrophic failure. The latter would happen for a bedrock with low roughness, which is less able to provide vestigial resistance to constrain ice velocity in case of failure in the till. We propose that the change in effective normal stress due to increasing pore pressure in the till beneath the temperate areas of the Aru glaciers quickly reduced the basal shear stress to the ultimate strength of glacier till. The glacier shape did not adjust fast enough to reduce the driving stress due to strain rate limitation in the cold-based areas producing large stresses in the remaining sticky spots (Figure 8) until their sudden rupture. The sticky spots are likely remnant of stiff frozen till rather that solid rock irregularities; rendering them rendering them susceptible to failure under high stress and vulnerable to thaw from water-

saturated temperate surrounding and increasing deformational heat. High clay and silt content measured in the till suggests low friction-angle properties (Iverson et al., 1998) and higher sensitivity of the shear strength to water pressure.

As one likely scenario for their development, the collapsed Aru glaciers probably grew in the past (pre-industrial climate) in colder conditions with low melting in summer allowing basal till stiffness to support high driving stress (see section 4.3). The low water pressure meant that actually there was likely very little sliding and very little production of till at that time. Upon commencement of some sliding, which may have occurred gradually over an increasing area of the bed over the past century, till was produced and the local glacier deformation regime tended to adapt to the distribution of till and liquid water reaching the bed. However, to continue the above scenario, the percolation into and accumulation of meltwater beneath the glaciers increased so rapidly in recent years that they could not keep balance with the changing conditions at the bed. Sliding may also contributed to increase water pressure in a positive feedback by destroying any efficient drainage system (Clarke et al., 1984). The contribury role of a soft-bed lithology in the collapses is therefore threefold by (i) behaving with plastic rheology when shear strength is reached, (ii) exhibiting low roughness and (iii) maintaining high water pressure while sliding speed increases; a known process that accounts for surge behaviour (Clarke et al., 1984; Fowler et al., 2001; Raymond, 1987). High content in clay and silt probably also lead to low hydraulic conductivity favourable to higher water pressure in the till (Fowler et al., 2001).

We believe that the existence of a high friction area in Aru-2 tongue prior to collapse is due to both, higher basal normal stresses (see supplementary material, Figure S2) increasing the till strength and higher lateral drags decreasing the basal shear stresses compared to Aru-1 (Figure 9). In this way, contrary to Aru-1, basal shear stress in the tongue area of Aru-2 only reached the ultimate shear strength of the till just before the final collapse in response to both decreasing resistance of the lateral margin and increasing driving stresses (due to bulging).

5.4. Till strength controlled glacier collapses

The Aru collapses (and in retrospective the Kolka Glacier collapse) define a new type of avalanching glaciers that are underlain by a failing substrate. Such “iceslides” could occur on fairly low angle glaciers, involving therefore large volumes of material and presenting serious consequences in terms of hazard potentials. The high sensitivity of the ultimate shear strength of the substrate to water pore pressure associated with low bed roughness allows for a dramatic and durable change of basal friction capable of driving this kind of instability.

The Kolka event in 2002 in the Caucasus Mountains is probably another example of this type of instability in which ultimate shear strength of the till is reached by a sudden increase of basal shear stress at constant effective normal stresses. Indeed, during the few weeks before this collapse, a significant mass had been added on top of the glacier by rock and ice fall activity increasing basal shear and normal stresses (Evans et al., 2009; Huggel et al., 2005). If the till was saturated with water and had low hydraulic conductivity, increasing water pore pressure could have compensated for the rising normal stress keeping the normal effective stress constant. The ultimate shear strength can be reached triggering the failure (Evans et al., 2009). This

hypothesis is realistic since Kolka glacier is known to be a surging glacier able to store large amounts of liquid water, and high water content and pressure were observed before its 2002 collapse (Kotlyakov et al., 2004).

However, changes in till-strength in response to water pressure are likely involved in surge mechanisms of temperate glaciers without the large majority of surges turning into gigantic collapses. This renders sudden changes in till strength as a necessary but not a fully sufficient condition for till-strength controlled collapses. The necessary second condition would be to maintain high driving stress even with low bed roughness while the till weakens. This means that the glacier has to grow over time atop a more stable substrate supporting higher driving stresses. In particular, freezing conditions allows for the development of a relatively thick glaciers on slopes that would else not be able to support such shear stress under the presence of liquid water. This makes the spatio-temporal interplay of soft-bed characteristics and polythermal regime a prerequisite of the Aru collapses. On-going climate change (i.e. warming) increases in many regions surface melt and the amount of water reaching glacier beds; modifying the till shear strength, and is therefore susceptible to drive more till-strength controlled collapses. The most impacted glaciers would be those flowing on soft and highly erodible bed lithologies at high driving stress, particularly those with heterogeneous thermal structure (polythermal glaciers). Such glaciers are mostly localized in cold and dry climates where a small increase in temperature results in a relatively large change in melting conditions such that the amount of water reaching the glacier base can significantly increase instability.

6. Conclusion

In summer 2016, one of the most spectacular glacier hazard events ever observed on glaciers occurred in Western Tibet. The twin collapse of Aru glaciers set a new reference in terms of size and mobility of glacier instabilities and requires revisiting our knowledge of impacts and hazards linked to glaciers in mountainous areas. Using 3D thermo-mechanical modelling together with satellite and field observations we conclude that the twin collapses were driven by increasing melt water reaching the bed in the temperate area of the glaciers polythermal structure of the glacier leading to the weakening of till and sediment underneath them .

Our steady-state simulation reveals that both glaciers are likely polythermal, with predominant temperate basal conditions over the detachment areas. Using satellite-observed elevation change and modeled surface mass balance, we reconstructed the frictional and shear stress regimes at the glacier base during the five years prior to collapse. We show that both glaciers experienced a stress transfer in their detachment area from basal drag to lateral shearing at the detachment margin that likely began around 2012. However, the different spatial repartitions of basal drag in the two detachment zones led to visibly different behaviours. As early as 2015, basal drag in the northern Aru-1 was very low over the whole detachment zone with a few remnant sticky spots where stress was concentrated. In contrast, basal drag of the southern Aru-2 was distributed between a low-friction area in the upper half of the detachment zone and a high-friction area in the lower half. These circumstances led to a progressive destabilization of Aru-1 with a significant acceleration in ice flow in the detachment zone over several years

prior to collapse whereas stresses accumulated in Aru-2 until a sudden break of the shear margin only few days before the collapse.

We interpret that the change in friction was due to glacier till reaching its ultimate shear strength in response to increasing water pore pressure. This assumption is supported by field observations showing soft and erodible material with high clay/silt content underneath the glaciers. Plastic rheology of the Aru glaciers till combined with low bedrock roughness and polythermal glacier structure seem to be the basis of the collapses. The polythermal structure enabled the glaciers to grow at high driving stress on a partially frozen substrate while temperate areas facilitated the water to reach the bed. Increasing water pressure in temperate areas led to failure in the till and thereby to increasing shear stresses on localized sticky spots and along the detachment margin. Due to the low bed roughness, the nature of these sticking spots seems purely thermal (cold patches). They are therefore mechanically breakable and can be affected by thermal effects such as intense deformational heat or latent heat release.

Under climatic changes and related increase in surface melt rates, polythermal glaciers underlain by soft and erodible substrate are likely to destabilize more readily than hard-bed glaciers due to lower bed roughness of the former, till plastic rheology, and hydrological feedbacks with high till shear rate in response of high water pressure and inefficient drainage system by destroying efficient drainage components (canals). The Aru cases highlight the most extreme of the plausible glacier behaviours when bedrock roughness is unable to achieve the global stability while substrate is failing, leading the catastrophic failure of large glacier sections.

Acknowledgements

We are grateful to the satellite data providers: CNES for Pleiades, Airbus/CNES for Spot 7, DLR for TanDEM-X, and Digital Globe for WorldView. A.K. and A.G. acknowledge the Univ. Oslo EarthFlows initiative and funding from the European Research Council under the European Union's Seventh Framework Programme (FP/2007-2013)/ERC grant agreement no. 320816, and A.K. also acknowledges the ESA projects Glaciers_cci (4000109873/14/I-NB) and DUE GlobPermafrost (4000116196/15/IN-B). S.G. acknowledges support from the French Space Agency (CNES) and the Programme National de Télédétection Spatiale grant PNTS-2016-01. A.G. acknowledges the Institute of Tibetan Plateau for organizing field trip in summer 2017 and M. S. Naoroz at the department of Geosciences, University of Oslo for his support with the samples analyses.

References

Aschwanden, A., Bueler, E., Khroulev, C. and Blatter, H.: An enthalpy formulation for glaciers and ice sheets, J. Glaciol., 58(209), 441–457, doi:10.3189/2012JoG11J088, 2012.

Bartholomaus, T. C., Anderson, R. S. and Anderson, S. P.: Response of glacier basal motion to transient water storage, Nat. Geosci., 1(1), 33–37, doi:10.1038/ngeo.2007.52, 2008.

Boulton, G. S. and Jones, A. S.: Stability of Temperate Ice Caps and Ice Sheets Resting on Beds of Deformable Sediment, J. Glaciol., 24(90), 29–43, doi:10.1017/S0022143000014623, 1979.

Clarke, G. K. C.: Subglacial Processes, Annu. Rev. Earth Planet. Sci., 33(1), 247–276, doi:10.1146/annurev.earth.33.092203.122621, 2005.

Clarke, G. K. C., Collins, S. G. and Thompson, D. E.: Flow, thermal structure, and subglacial conditions of a surge-type glacier, Can. J. Earth Sci., 21(2), 232–240, doi:10.1139/e84-024, 1984.

Cuffey, K. M. and Paterson, W. S. B.: The physics of glaciers, 4th ed., Academic Press, Amsterdam. [online] Available from: https://books.google.ca/books?hl=en&lr=&id=Jca2v1u1EKEC&oi=fnd&pg=PP2&dq=cuffey+and+paterson&ots=KLIT65smg9&sig=B_157C4FSC4Doh3mWznzjKJr5pY (Accessed 27 November 2015), 2010.

Evans, S. G., Tutubalina, O. V., Drobyshev, V. N., Chernomorets, S. S., McDougall, S., Petrakov, D. A. and Hungr, O.: Catastrophic detachment and high-velocity long-runout flow of Kolka Glacier, Caucasus Mountains, Russia in 2002, Geomorphology, 105(3), 314–321, doi:10.1016/j.geomorph.2008.10.008, 2009.

Faillettaz, J., Funk, M. and Vincent, C.: Avalanching glacier instabilities: Review on processes and early warning perspectives, Rev. Geophys., 53, doi:10.1002/2014RG000466., 2015.

Farr, T. G., Rosen, P. A., Caro, E., Crippen, R., Duren, R., Hensley, S., Kobrick, M., Paller, M., Rodriguez, E., Roth, L., Seal, D., Shaffer, S., Shimada, J., Umland, J., Werner, M., Oskin, M., Burbank, D. and Alsdorf, D.: The Shuttle Radar Topography Mission, Rev. Geophys., 45(2), n/a-n/a, doi:10.1029/2005RG000183, 2007.

Fowler, A. C., Murray, T. and Ng, F. S. L.: Thermally controlled glacier surging, J. Glaciol., 47(159), 527–538, doi:10.3189/172756501781831792, 2001.

Gagliardini, O., Zwinger, T., Gillet-Chaulet, F., Durand, G., Favier, L., De Fleurian, B., Greve, R., Malinen, M., Martín, C., R\a aback, P. and others: Capabilities and performance of Elmer/Ice, a new-generation ice sheet model, Geosci. Model Dev., 6(4), 1299–1318, doi:10.5194/gmd-6-1299-2013, 2013.

Gilbert, A., Gagliardini, O., Vincent, C. and Wagnon, P.: A 3-D thermal regime model suitable for cold accumulation zones of polythermal mountain glaciers, J. Geophys. Res., 119(9), 1876–1893, doi:10.1002/2014JF003199, 2014.

Gilbert, A., Vincent, C., Gagliardini, O., Krug, J. and Berthier, E.: Assessment of thermal change in cold avalanching glaciers in relation to climate warming, Geophys. Res. Lett., 42(15), 6382–6390, doi:10.1002/2015GL064838, 2015.

Gilbert, A., Flowers, G. E., Miller, G. H., Rabus, B. T., Van Wychen, W., Gardner, A. S. and Copland, L.: Sensitivity of Barnes Ice Cap, Baffin Island, Canada, to climate state and internal dynamics, J. Geophys. Res. Earth Surf., 121(8), 1516–1539, doi:10.1002/2016JF003839, 2016.

Gillet-Chaulet, F., Gagliardini, O., Seddik, H., Nodet, M., Durand, G., Ritz, C., Zwinger, T., Greve, R. and Vaughan, D. G.: Greenland ice sheet contribution to sea-level rise from a new-generation ice-sheet model, The Cryosphere, 6(6), 1561–1576, doi:10.5194/tc-6-1561-2012, 2012.

Huggel, C., Zgraggen-Oswald, S., Haeberli, W., Kääb, A., Polkvoj, A., Galushkin, I. and Evans, S. G.: The 2002 rock/ice avalanche at Kolka/Karmadon, Russian Caucasus: assessment of extraordinary avalanche formation and mobility, and application of QuickBird satellite imagery, Nat. Hazards Earth Syst. Sci., 5(2), 173–187, 2005.

Iverson, N. R.: Shear resistance and continuity of subglacial till: hydrology rules, J. Glaciol., 56(200), 1104–1114, 2010.

Iverson, N. R., Hooyer, T. S. and Baker, R. W.: Ring-shear studies of till deformation: Coulomb-plastic behavior and distributed strain in glacier beds, J. Glaciol., 44(148), 634–642, doi:10.1017/S0022143000002136, 1998.

Joughin, I., MacAyeal, D. R. and Tulaczyk, S.: Basal shear stress of the Ross ice streams from control method inversions, J. Geophys. Res. Solid Earth, 109(B9), B09405, doi:10.1029/2003JB002960, 2004.

Kääb, A., Leinss, S., Gilbert, A., Bühler, Y., Gascoin, S., Evans, S. G., Bartelt, P., Berthier, E., Brun, F., Chao, W.-A., Farinotti, D., Gimbert, F., Guo, W., Huggel, C., Kargel, J. S., Leonard, G. J., Tian, L., Treichler, D. and Yao, T.: Massive collapse of two glaciers in western Tibet in 2016 after surge-like instability, Nat. Geosci., 11(2), 114–120, doi:10.1038/s41561-017-0039-7, 2018.

Kotlyakov, V. M., Rototaeva, O. V. and Nosenko, G. A.: The September 2002 Kolka Glacier Catastrophe in North Ossetia, Russian Federation: Evidence and Analysis, Mt. Res. Dev., 24(1), 78–83, doi:10.1659/0276-4741(2004)024[0078:TSKGCI]2.0.CO;2, 2004.

Krug, J., Weiss, J., Gagliardini, O. and Durand, G.: Combining damage and fracture mechanics to model calving, The Cryosphere, 8(6), 2101–2117, doi:10.5194/tc-8-2101-2014, 2014.

Lliboutry, L.: General theory of subglacial cavitation and sliding of temperate glaciers, J. Glaciol., 7, 21–58, 1968.

MacAyeal, D. R.: The basal stress distribution of Ice Stream E, Antarctica, inferred by control methods, J. Geophys. Res. Solid Earth, 97(B1), 595–603, doi:10.1029/91JB02454, 1992.

Minchew, B., Simons, M., Björnsson, H., Pálsson, F., Morlighem, M., Seroussi, H., Larour, E. and Hensley, S.: Plastic bed beneath Hofsjökull Ice Cap, central Iceland, and the sensitivity of ice flow to surface meltwater flux, J. Glaciol., 62(231), 147–158, doi:10.1017/jog.2016.26, 2016.

van Pelt, W. J. J., Oerlemans, J., Reijmer, C. H., Pettersson, R., Pohjola, V. A., Isaksson, E. and Divine, D.: An iterative inverse method to estimate basal topography and initialize ice flow models, The Cryosphere, 7(3), 987–1006, doi:10.5194/tc-7-987-2013, 2013.

Pralong, A. and Funk, M.: Dynamic damage model of crevasse opening and application to glacier calving, J. Geophys. Res. Solid Earth 1978–2012, 110(B1), doi:10.1029/2004JB003104, 2005.

Raymond, C. F.: How do glaciers surge? A review, J. Geophys. Res. Solid Earth, 92(B9), 9121–9134, doi:10.1029/JB092iB09p09121, 1987.

Schoof, C.: Ice-sheet acceleration driven by melt supply variability, Nature, 468(7325), 803–806, doi:10.1038/nature09618, 2010.

Stokes, C. R., Clark, C. D., Lian, O. B. and Tulaczyk, S.: Ice stream sticky spots: A review of their identification and influence beneath contemporary and palaeo-ice streams, Earth-Sci. Rev., 81(3), 217–249, doi:10.1016/j.earscirev.2007.01.002, 2007.

Tao, W. and Shen, Z.: Heat flow distribution in Chinese continent and its adjacent areas, Prog. Nat. Sci., 18(7), 843–849, doi:10.1016/j.pnsc.2008.01.018, 2008.

Thompson, L. G., Mosley-Thompson, E., Davis, M. E., Lin, P. N., Dai, J., Bolzan, J. F. and Yao, T.: A 1000 Year Climate Ice-Core Record from the Guliya Ice Cap, China: Its Relationship to Global Climate Variability, Ann. Glaciol., 21(1), 175–181, doi:10.3198/1995AoG21-1-175-181, 1995.

Tian, L., Yao, T., Gao, Y., Thompson, L., Mosley-Thompson, E., Muhammad, S., Zong, J., Wang, C., Jin, S. and Li, Z.: Two glaciers collapse in western Tibet, J. Glaciol., 1–4, doi:10.1017/jog.2016.122, 2016.

Truffer, M., Echelmeyer, K. A. and Harrison, W. D.: Implications of till deformation on glacier dynamics, J. Glaciol., 47(156), 123–134, 2001.

Tsai, V. C., Stewart, A. L. and Thompson, A. F.: Marine ice-sheet profiles and stability under Coulomb basal conditions, J. Glaciol., 61(226), 205–215, doi:10.3189/2015JoG14J22, 2015.

Vincent, C. and Moreau, L.: Sliding velocity fluctuations and subglacial hydrology over the last two decades on Argentière glacier, Mont Blanc area, J. Glaciol., 62(235), 805–815, doi:10.1017/jog.2016.35, 2016.

Voight, B.: Materials science laws applies to time forecast of slope failure, in Proceedings 5th International Symposium on Landslides, Lausanne 1988, vol. 3, pp. 1471–1472, C. Bonnard, A. A. Balkema, Lisse, Netherlands., 1990.

Weertman, J.: The theory of glacier sliding, J. Glaciol., 5(39), 287–303, 1964.

The Cryosphere Discuss., https://doi.org/10.5194/tc-2018-45
Manuscript under review for journal The Cryosphere
Discussion started: 15 March 2018

Table 1 – Different DEMs used in this study from satellite imagery

Satellite /Sensor	Acquisition date	Resolution	Image type
SRTM C/X	February 2000	30 m	Radar
TanDEM-X	6 June 2011	10 m	Radar
TanDEM-X	14 April 2013	10 m	Radar
TanDEM-X	01 April 2014	10 m	Radar
Spot7	06 September 2015	5 m	Optical
Worldview	25 November 2015	5 m	Optical
Pléiades	01 October 2016	5 m	Optical

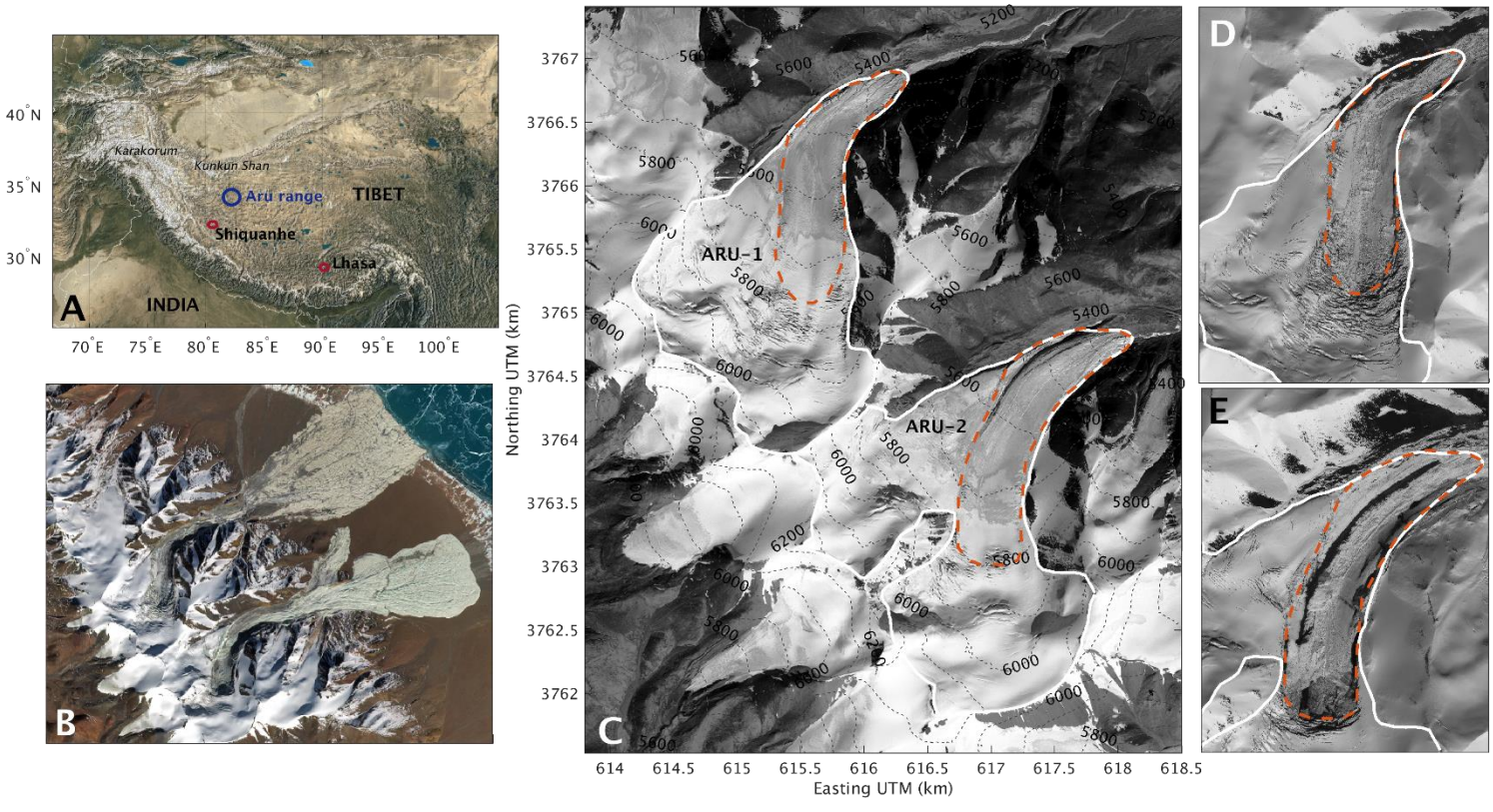

Figure 1 – (A) Location of the Aru range in Tibet and (B) Sentinel-2 image from 2016, December 8 after the collapses. (C) Topographic map of Aru-1 and Aru-2 (vertical datum WGS84) with an orthorectified Airbus Spot7 image from 2015 September 21 as background; orange dashed lines indicate the detachment outline, white lines are the glacier outline as of 2015. (D, E) Pléiades images from 2016, October 1 of the two glaciers Aru-1 (D) and Aru-2 (E) after the collapses.

The Cryosphere Discuss., https://doi.org/10.5194/tc-2018-45
Manuscript under review for journal The Cryosphere
Discussion started: 15 March 2018

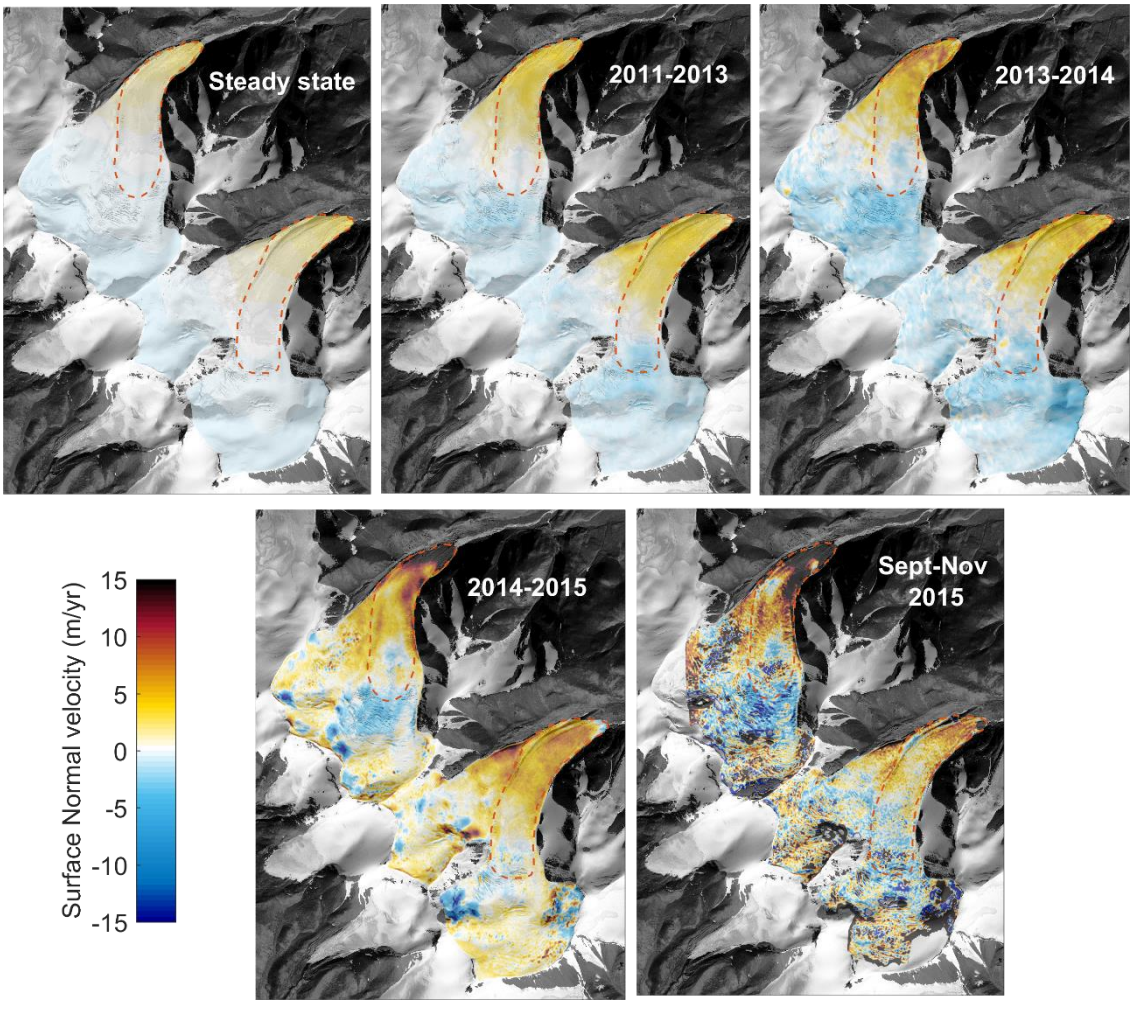

Figure 2 – Mean vertical component of the surface-normal velocities obtained by DEM comparison and mass balance modeling during different periods prior to the collapse. Steady-state velocities in the first panel are modeled.

The Cryosphere Discuss., https://doi.org/10.5194/tc-2018-45
Manuscript under review for journal The Cryosphere
Discussion started: 15 March 2018

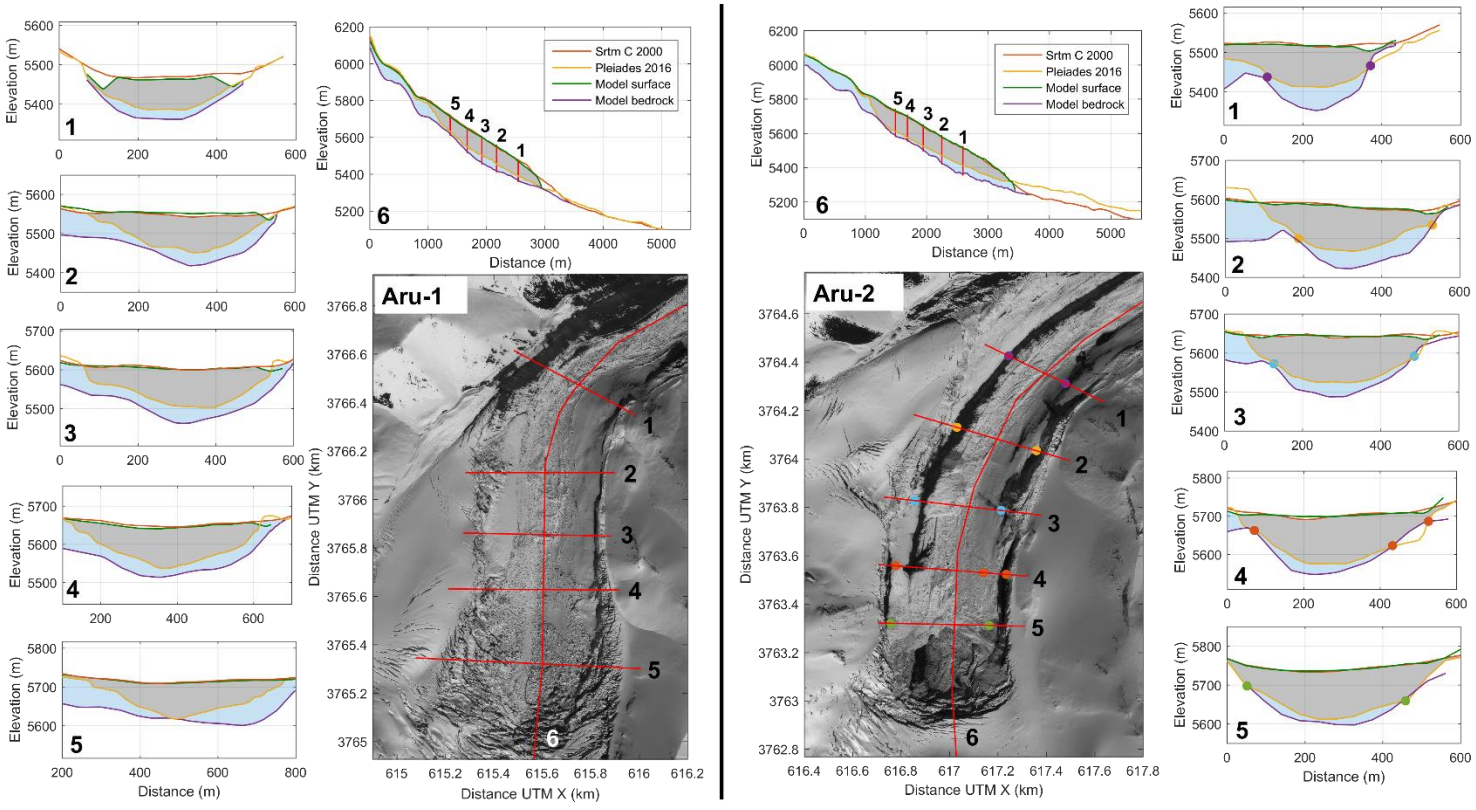

Figure 3 – Pléiades image of Aru-1 (left) and 2 (right) after collapse with topographic profiles 1 to 6 plotted for both glaciers. The topographic profiles 1 to 6 show the measured surface topography in 2000 (SRTM, in red) and 2016 after the collapse (Pléiades, in yellow). These profiles are compared with the modeled bedrock (in purple) and surface (in green) topography. The colored dots on Aru 2 show the location of specific points of the profiles in the Pléiades image: those points correspond to locations where our reconstruction matches the Pléiades DEM and where bedrock should thus visible on the Pléiades image (no ice debris). Grey shading indicates the detached areas according to the Pléiades DEM.

The Cryosphere Discuss., https://doi.org/10.5194/tc-2018-45
Manuscript under review for journal The Cryosphere
Discussion started: 15 March 2018

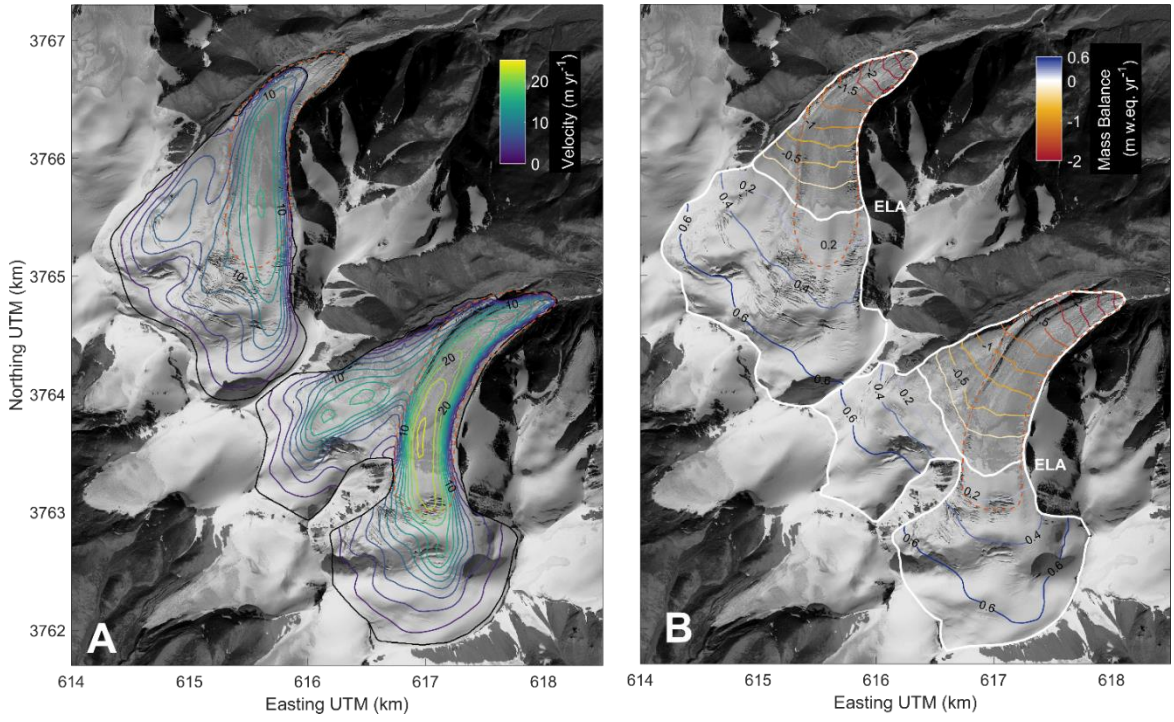

Figure 4 – Modeled steady-state horizontal surface velocities (A) and surface mass balance (B) for Aru-1 and Aru-2. The black contours in (A) are modeled steady-state glacier outlines. The white contour in (B) is the glacier outline as in 2015.

The Cryosphere Discuss., https://doi.org/10.5194/tc-2018-45
Manuscript under review for journal The Cryosphere
Discussion started: 15 March 2018

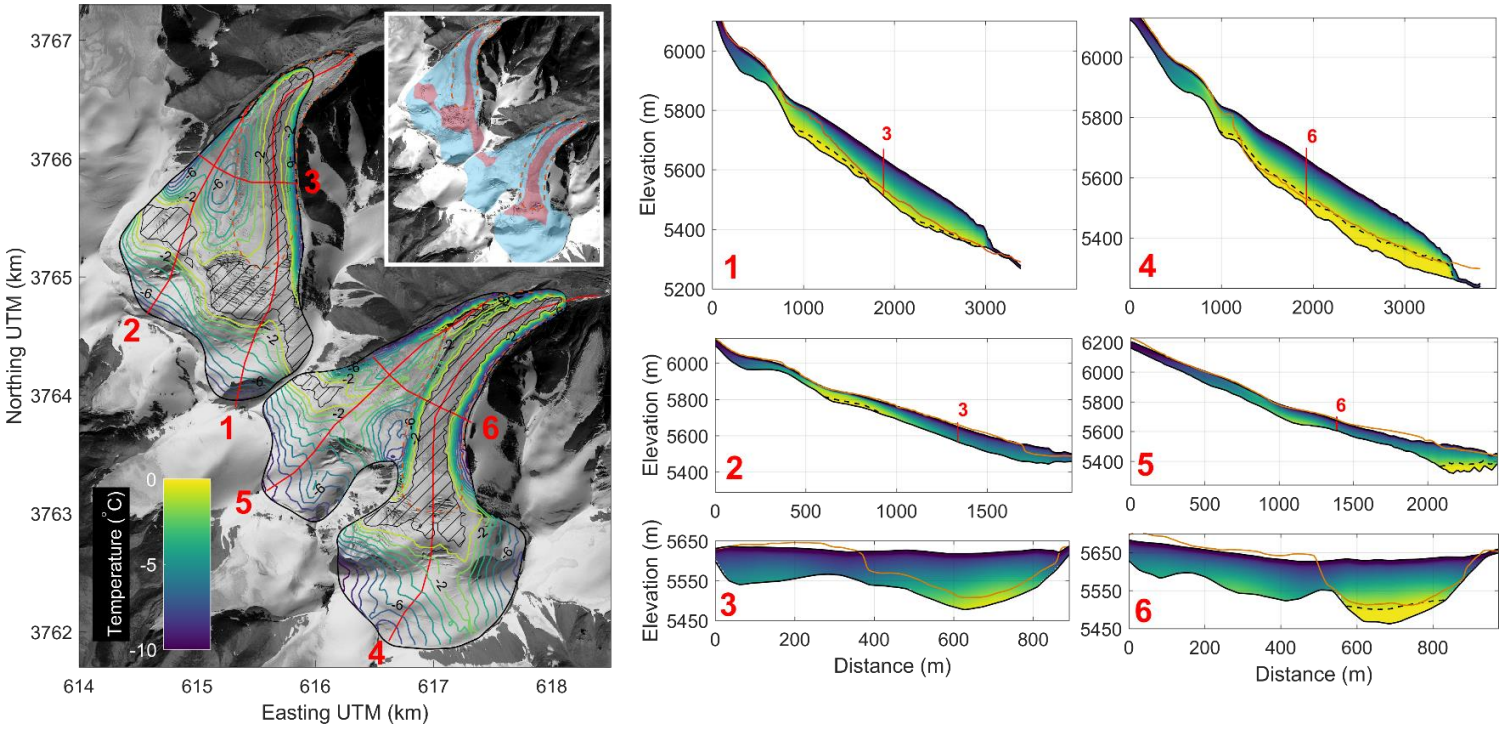

Figure 5 - Modeled steady state temperature on Aru-1 and Aru-2. Left panel shows basal temperature where black hatched lines are temperate areas with an inset figure highlighting temperate-based (red) and cold-based (blue) areas. Right panels show 2D temperature profiles 1 to 6 as indicated in the left panel (red lines). Profiles include Pleiades 2016 elevation profiles (orange lines). The dashed black lines indicate the cold-temperate transition surface. Note that vertical scale is exaggerated in profiles 1 and 4.

The Cryosphere Discuss., https://doi.org/10.5194/tc-2018-45
Manuscript under review for journal The Cryosphere
Discussion started: 15 March 2018

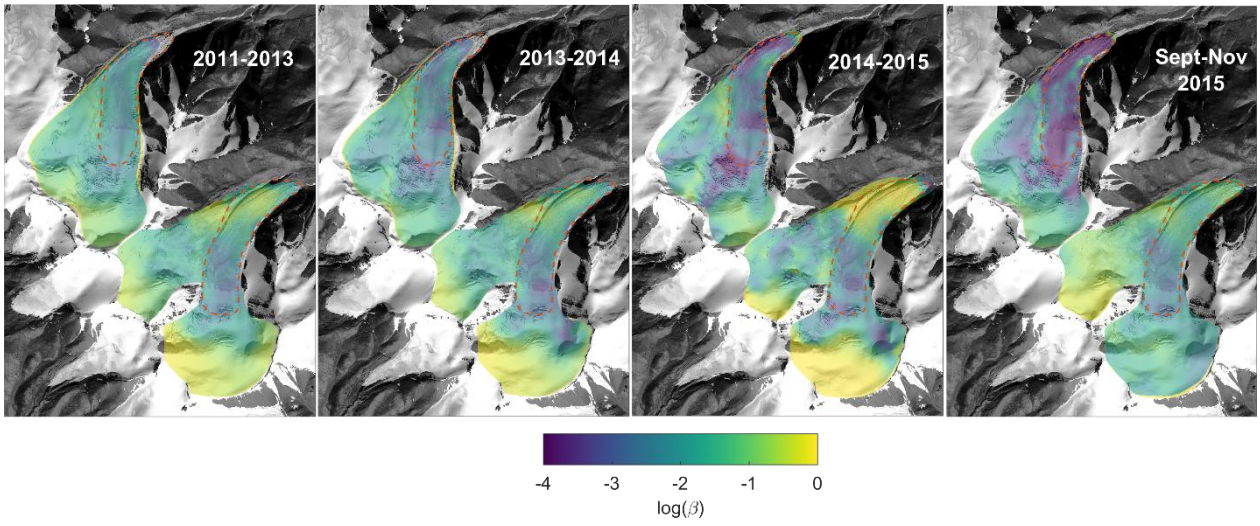

Figure 6 - Friction coefficient β inferred from surface-normal velocity during different periods prior to the collapse.

The Cryosphere Discuss., https://doi.org/10.5194/tc-2018-45
Manuscript under review for journal The Cryosphere
Discussion started: 15 March 2018

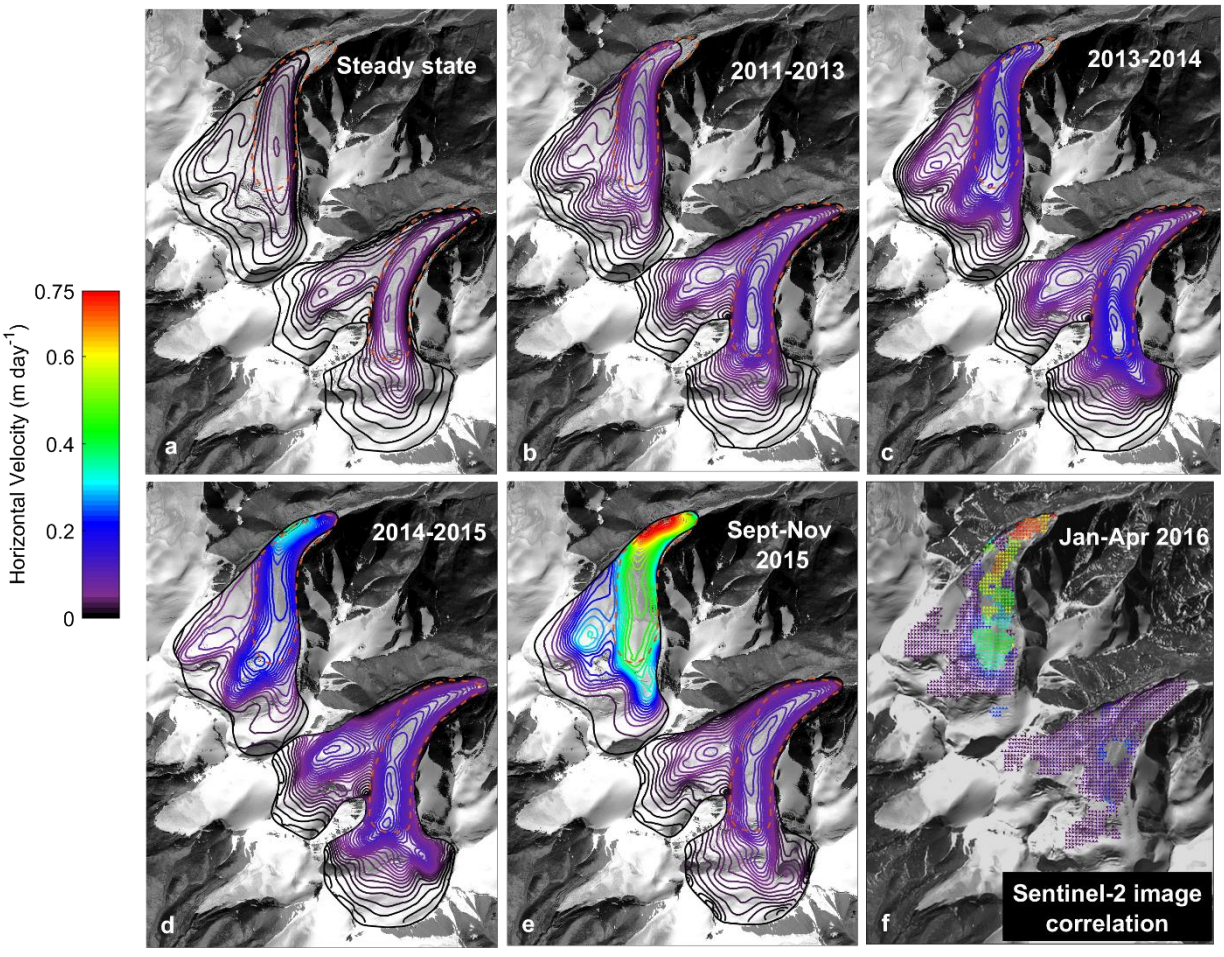

Figure 7 – (a-e) Modeled mean horizontal velocities for the two glaciers at steady state and for the period 2011-2013, 2013-2014, 2014-2015 and September to November 2015. (f) Measured horizontal velocities from Sentinel-2 image correlation between January and April 2016

The Cryosphere Discuss., https://doi.org/10.5194/tc-2018-45
Manuscript under review for journal The Cryosphere
Discussion started: 15 March 2018

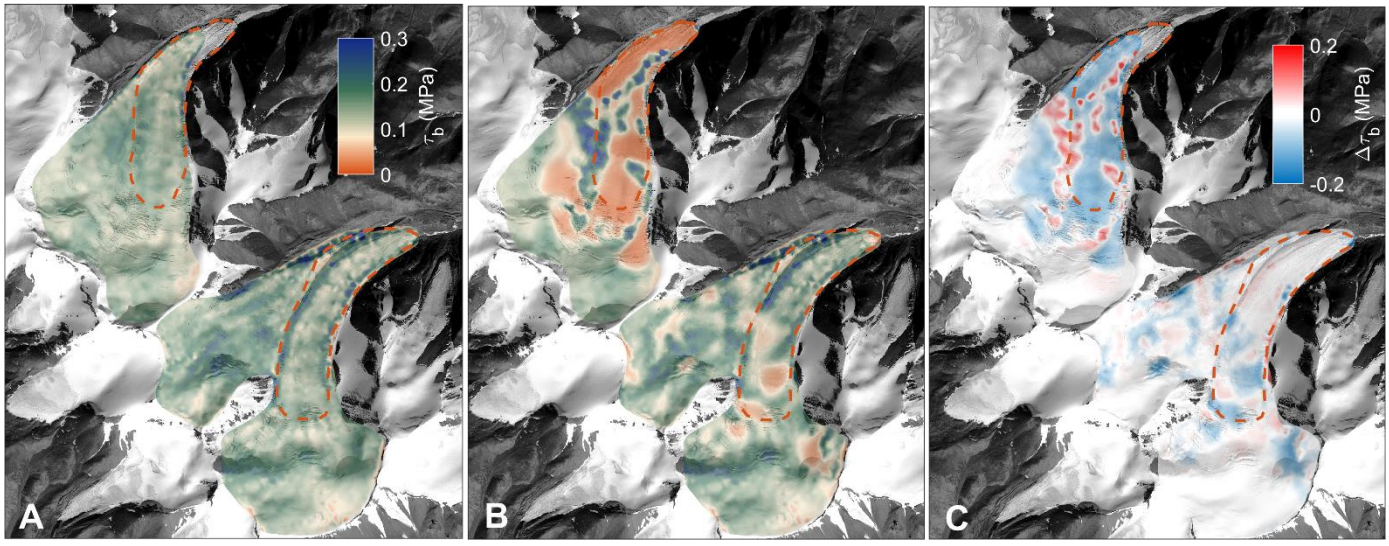

Figure 8 – Modeled basal shear stress at steady state (A) and in November 2015 (B). (C) is the difference between (A) and (B).

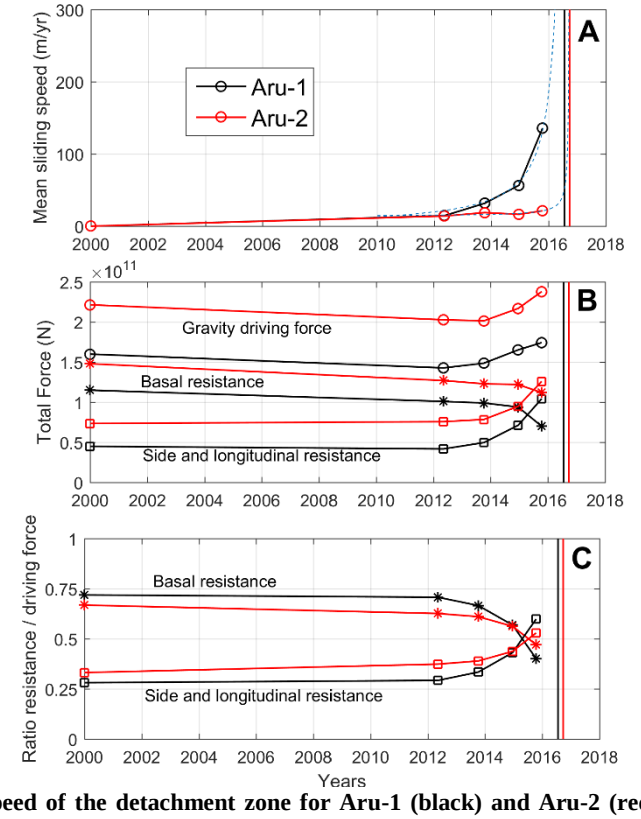

Figure 9 – (A) Mean sliding speed of the detachment zone for Aru-1 (black) and Aru-2 (red). The dashed blue lines show predicted speed following an empirical law of slope failure [Voight, 1990]. (B) Force balance of the detachment along the glacier bed direction. (C) Ratio of resisting force over driving force. Vertical lines show collapse dates in the three panels.

The Cryosphere Discuss., https://doi.org/10.5194/tc-2018-45
Manuscript under review for journal The Cryosphere
Discussion started: 15 March 2018

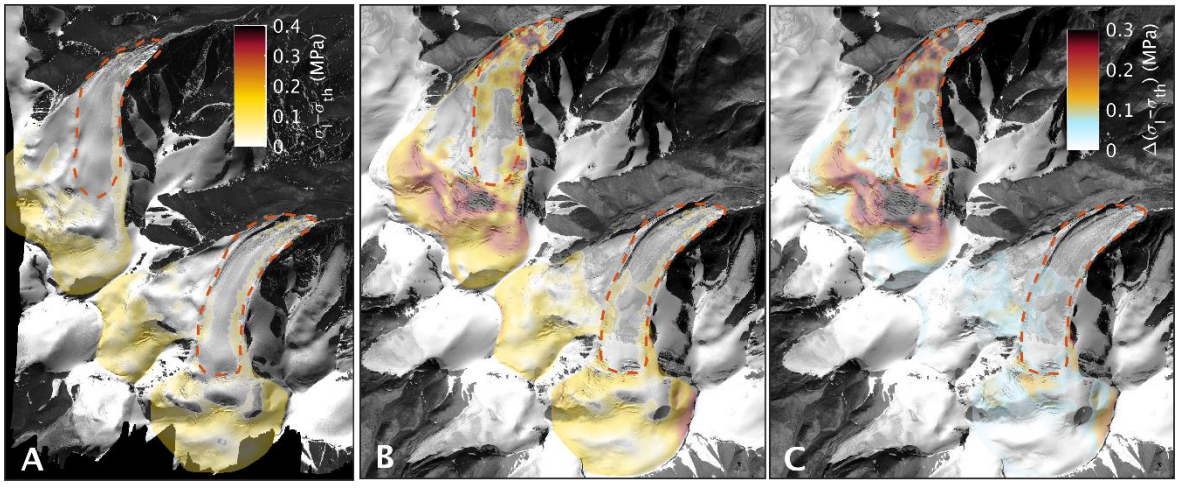

Figure 10 – Maximum principal Cauchy stress excess above damage initiation threshold at steady state (A) and prior to collapse (B) at the glacier surface. (C) shows the difference between (A) and (B). Background image in (A) is a WorldView image from 2011, December 2 when the instability just started. Background image in (B) and (C) is a Spot 7 image from 2015 September 21, one year before collapse. These results show a good match between predicted and observed crevasse formation in response to frictional changes.

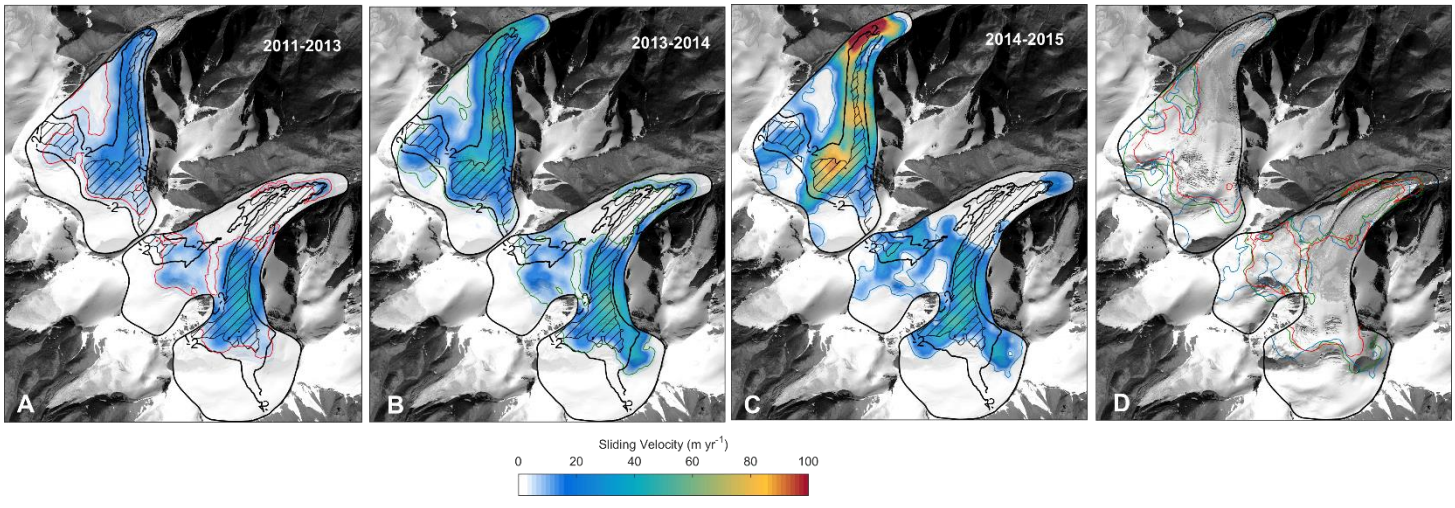

Figure 11 – (A, B, C) Modeled temperate area (hatched zones) and -2°C isotherm at steady state compared with sliding speeds over different periods (background colormap). (D) Comparison of sliding location for the different periods.

5

The Cryosphere Discuss., https://doi.org/10.5194/tc-2018-45
Manuscript under review for journal The Cryosphere
Discussion started: 15 March 2018

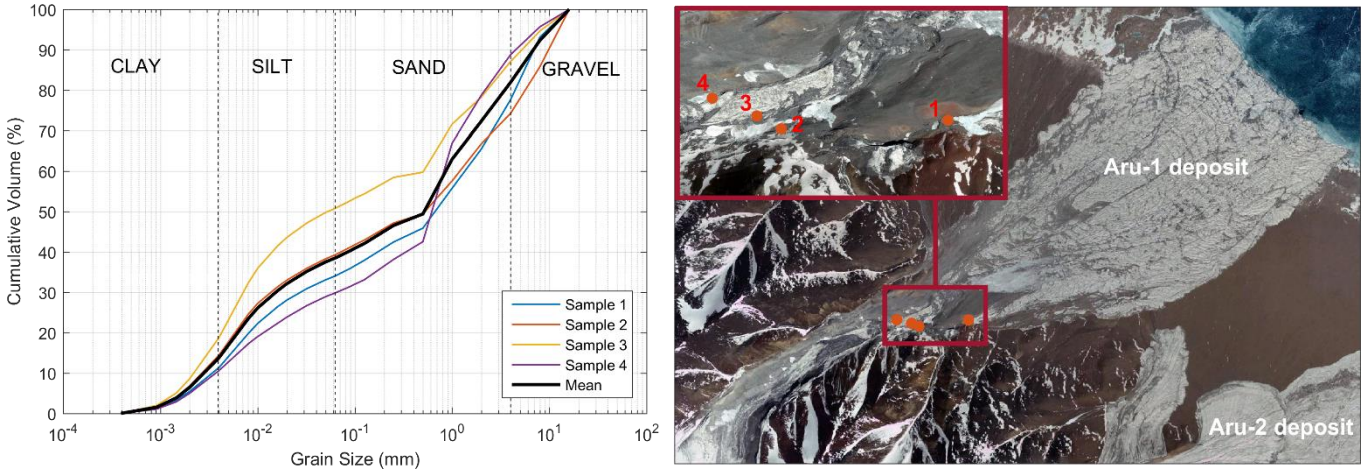

Figure 12 – Grain-size distribution measured in four glacier till samples collected in the Aru-1 deposit area (numbers 1 to 4 in the right panel).